Extreme Mechanics Letters 6 (2016) 10–22

Contents lists available at ScienceDirect

Extreme Mechanics Letters

journal homepage: www.elsevier.com/locate/eml

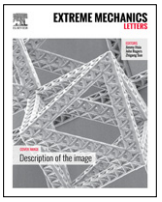

On modeling of fractured media using an enhanced embedded discontinuity approach

E. Haghighat *, S. Pietruszczak

Department of Civil Engineering, McMaster University, Hamilton, Ontario, Canada

ARTICLE INFO

Article history:
Received 24 July 2015
Received in revised form 29 September 2015
Accepted 13 November 2015
Available online 17 November 2015

Keywords:
Discrete crack propagation
Embedded discontinuity
Extended FEM
Constitutive modeling

ABSTRACT

The main focus of this study is on application of the enhanced embedded discontinuity approach to the analysis of pre-existing fractures. The J-integral is used to evaluate the energy release rate around the crack tip and its value is compared with both that obtained from Extended FEM simulations as well as from an analytical solution. The approach is also used for modeling of cohesive crack propagation. It is demonstrated that the framework gives results that are very close to those obtained using Extended FEM, while the former requires less computational effort. A comparison with a standard smeared approach is provided in order to highlight the nature of the contribution. The embedded discontinuity framework is also applied to flow problems with pre-existing cracks. A modified form of Fourier law is introduced and later employed for modeling of heat transfer/flow in the domain that contains thermally isolated/impervious cracks.

1. Introduction

This study is an extension of earlier work reported in [1]. The main objective here is to investigate the accuracy (in relation to XFEM) of the approach incorporating an enhanced constitutive law with embedded discontinuity for the analysis of crack propagation. In addition, using a similar methodology, a new modified form of Fourier law is introduced that is capable of describing flow within the domain containing thermally/hydraulically isolated inclusions. A number of numerical examples are provided addressing both of the above issues.

Modeling of damage initiation and propagation has been one the most intensely researched topics over the last few decades. The existing analytical solutions are restricted to an elastic material and involve simple geometries and boundary conditions. Therefore, they are not directly relevant to practical engineering problems. The latter require, in general, a numerical simulation that typically involves the use of the Finite Element Method (FEM). The early methodologies for capturing the progressive damage were based on tracing the crack propagation on the element boundaries [2]. These were later combined with remeshing techniques [3] to increase the accuracy of the simulated crack pattern. In addition, some smeared techniques have also been proposed that incorporated plasticity-based strain-softening relations [4,5]. A detailed review of early FEM-based methodologies for crack propagation analysis can be found in [6]. The concept of enhancing the standard strain-softening frameworks to ensure the mesh-independency was first presented in Ref. [7]. The approach advocates the use of volume averaging to estimate the properties of an initially homogeneous medium intercepted by a shear band/interface. The proposed constitutive relation incorporates the properties of constituents (viz. intact material and interface) as well as a characteristic dimension associated with the structural arrangement, which provides a length scale in the constitutive model. The issue of analysis of strong discontinuities induced by strain softening was later addressed in [8]. In that study,

* Corresponding author.
E-mail address: haghige@mcmaster.ca (E. Haghighat).

http://dx.doi.org/10.1016/j.eml.2015.11.001
2352-4316/

a description of discontinuous motion was introduced, via an enriched strain field, and was incorporated into the finite element interpolants [9]. After introduction of the partition of unity approach [10], the Extended Finite Element Method (XFEM) was proposed [11,12], which allows not only for an accurate description of a discontinuous velocity/displacement field but also for incorporation of the tip enrichments into the approximation space. Although some conceptual similarities can be found between the strong discontinuity approach introduced in [8] and the XFEM, the latter provides a more elaborate way of incorporating any kind of asymptotic function into the FEM approximation space. The XFEM approach has been applied to various problems such as cohesive crack problem [13], frictional contact [14], strain localization [15,16], interface and fracture propagation in multi-phase media [17–19]. A detailed literature review can be found in [20]. The primary difficulty in implementing XFEM is the need to deal with additional degrees of freedom. In particular, a special treatment for activating enriched DOFs is required that generally increases the computational effort compared with the standard FEM. The main advantage of this method is the ability to incorporate any asymptotic function in the discretized model.

There are two key topics that can be addressed within XFEM, i.e. modeling of discontinuous motion by enriching the FE interpolants, and a discrete representation of crack. The latter results in a stable approach for advancing the analysis past the ultimate load that triggers the failure. This is in contrast with smeared crack models in which crack can initiate during equilibrium iterations and may form in the adjacent integration points. In discrete representation, the crack direction is fixed within an element and is identified after equilibrium iterations. In this way, the crack formation in two adjacent elements is usually avoided. The crack geometry is defined by the level-set method [21], which provides a smooth propagation path. It is believed here that a discrete representation of crack can result in a more stable algorithm for most smeared damage/crack models. In the recent study by authors [1], a discrete tracing of crack path was used as the key idea along with embedded discontinuity model [7,22] for modeling of both the cohesive crack propagation and strain localization. It was shown that the discrete representation improves the stability of the solution and results in similar global and local stress/strain distribution. A new procedure for deriving the governing equations was provided based on the general description of discontinuous motion. The approach was also used for the modeling of failure in anisotropic media [23]. The methodology employs some concepts originating from XFEM, such as discrete crack propagation strategies and level-set method; in terms of formulation, however, it is based on an enhanced plasticity/damage framework. As a result, a special treatment of elements that involves activating enrichments/distinct integration scheme for XFEM or static condensation in strong discontinuity approach, is no longer required.

The present paper is organized as follows. In the next section, the formulation for both XFEM as well as the standard FEM incorporating a constitutive law with embedded discontinuity (FEM/CLED) is outlined. The section is concluded by presenting an extension of CLED methodology to modeling of discontinuities in scalar field problems. This involves a modified version of Fourier law that can be employed for the analysis of heat transfer/fluid flow problems within domains containing discrete fractures. In Section 3, the procedure for tracing the propagation of crack path is addressed. In Section 4, the numerical simulations of traction free crack are provided, which include the evaluation of J-integral [24]. It is shown that both FEM/CLED and XFEM with Heaviside enrichment, i.e. no singular tip enrichment, result in almost identical energy release rates and stress/strain distribution. In Section 5, the results of numerical analysis of some selected problem involving cohesive crack propagation are addressed and the predictions are compared with experimental benchmarks. The study closes with an analysis involving a heat transfer within a domain containing a set of thermally non-conductive cracks of a random orientation. The results of both mechanical and flow simulations presented here clearly demonstrate that the FEM/CLED framework can be applied to a broad range of problems involving the presence of discontinuities.

2. Description of a discontinuous motion

Following Ref. [1], a discontinuous motion $\mathbf{v}(\mathbf{x}, t)$ in the domain Ω that contains a discontinuity surface Γ_d can be defined as

$$\mathbf{v}(\mathbf{x}, t) = \hat{\mathbf{v}}(\mathbf{x}, t) + \mathcal{H}_{\Gamma_d}\tilde{\mathbf{v}}(\mathbf{x}, t) \tag{1}$$

where, $\hat{\mathbf{v}}(\mathbf{x}, t)$ and $\tilde{\mathbf{v}}(\mathbf{x}, t)$ are continuous functions in the solution domain Ω and $\mathcal{H}_{\Gamma_d} = \mathcal{H}(\phi)$ is the Heaviside step function that can be expressed in its symmetric form as

$$\mathcal{H}(\phi) = 2\int_{-\infty}^{\phi} \delta(\varphi)\, d\varphi - 1 = \begin{cases} +1 & \phi > 0 \\ -1 & \phi \leq 0. \end{cases} \tag{2}$$

Here, $\phi = \phi(\mathbf{x})$ is the signed distance from the discontinuity interface Γ_d, and $\delta(\varphi)$ is the Dirac delta function which is defined as being singular at $\phi = 0$ and equal to zero elsewhere. Denoting jump of a function on the discontinuity interface by $[\![\bullet]\!] = \bullet^+ - \bullet^-$, the rate of separation between the opposite crack faces, i.e. $\dot{\mathbf{g}}$, can be defined as

$$\dot{\mathbf{g}} = [\![\mathbf{v}]\!] = \left(\hat{\mathbf{v}} + \mathcal{H}_{\Gamma_d}\tilde{\mathbf{v}}\right)^+ - \left(\hat{\mathbf{v}} + \mathcal{H}_{\Gamma_d}\tilde{\mathbf{v}}\right)^- = \hbar\,\tilde{\mathbf{v}}$$
$$\hbar = [\![\mathcal{H}]\!] = \mathcal{H}^+ - \mathcal{H}^- \tag{3}$$

where, based on the representation (2), the jump in the step function is $\hbar = 2$. Considering that $\nabla\mathcal{H}(\phi) = \mathcal{H}'\,\nabla\phi$ and $\mathcal{H}'(\phi) = \hbar\delta(\phi) = \hbar\delta_{\Gamma_d}$, the velocity gradient of the discontinuous motion (1) can be expressed as

$$\nabla^s\mathbf{v} = \nabla^s\hat{\mathbf{v}} + \mathcal{H}_{\Gamma_d}\nabla^s\tilde{\mathbf{v}} + \delta_{\Gamma_d}(\hbar\tilde{\mathbf{v}} \otimes \mathbf{n})^s \tag{4}$$

where $\mathbf{n} = \nabla\phi$ is the normal to the interface, and the superscript s refers to the symmetric part of the gradient operator.

2.1. Space discretization for XFEM strategy

Within the XFEM strategy, a discontinuous field can be incorporated into the approximation space by introducing enrichment functions and additional degrees of freedoms. Thus, the discontinuous motion (1) can be approximated

by

$$\begin{aligned}\mathbf{v}^h(\mathbf{x},t) &= \hat{\mathbf{v}}^h(\mathbf{x},t) + \mathcal{H}_{\Gamma_d}\tilde{\mathbf{v}}^h(\mathbf{x},t)\\ &= \hat{\mathbf{N}}(\mathbf{x})\dot{\hat{\mathbf{d}}}(t) + \mathcal{H}_{\Gamma_d}\tilde{\mathbf{N}}(\mathbf{x})\dot{\tilde{\mathbf{d}}}(t) = \mathbf{N}(\mathbf{x})\dot{\tilde{\mathbf{d}}}(t)\end{aligned} \tag{5}$$

where, $\hat{\mathbf{N}}$ and $\tilde{\mathbf{N}}$ are standard finite element shape functions that may have different orders of approximation and $\hat{\mathbf{d}}$ and $\tilde{\mathbf{d}}$ are standard and enriched degrees of freedom, respectively. In order to achieve a better representation of the enriched approximation and to avoid the use of blending elements, the shifted form of approximation (5) can be employed [25], viz.

$$\mathbf{v}^h(\mathbf{x},t) = \hat{\mathbf{N}}(\mathbf{x})\dot{\hat{\mathbf{d}}}(t) + \tilde{\mathbf{N}}(\mathbf{x})\boldsymbol{\Psi}(\mathbf{x})\dot{\tilde{\mathbf{d}}}(t) = \mathbf{N}(\mathbf{x})\dot{\tilde{\mathbf{d}}}(t). \tag{6}$$

Here, $\boldsymbol{\Psi}(\mathbf{x})$ is the shifted form of the step function defined as

$$\boldsymbol{\Psi}(\mathbf{x}) = \begin{bmatrix} \mathcal{H}(\phi)-\mathcal{H}(\phi_1) & 0 & \dots & 0 \\ 0 & \mathcal{H}(\phi)-\mathcal{H}(\phi_2) & \dots & 0 \\ \vdots & \vdots & \ddots & \vdots \\ 0 & 0 & \dots & \mathcal{H}(\phi)-\mathcal{H}(\phi_n) \end{bmatrix} \tag{7}$$

and n is the number of interpolation functions. Note that since $[\![\boldsymbol{\Psi}(\mathbf{x})]\!] = (\mathcal{H}^+ - \mathcal{H}^-)\,\mathbf{I} = \hbar\,\mathbf{I}$, where $\mathbf{I}$ is the identity matrix, the crack opening $\dot{\mathbf{g}}^h(\mathbf{x},t)$ can be expressed as

$$\begin{aligned}\dot{\mathbf{g}}^h(\mathbf{x},t) &= [\![\mathbf{v}^h(\mathbf{x},t)]\!] = [\![\hat{\mathbf{N}}(\mathbf{x})]\!]\dot{\hat{\mathbf{d}}}(t) + [\![\tilde{\mathbf{N}}(\mathbf{x})\boldsymbol{\Psi}(\mathbf{x})]\!]\dot{\tilde{\mathbf{d}}}(t)\\ &= \hbar\tilde{\mathbf{N}}(\mathbf{x})\dot{\tilde{\mathbf{d}}}(t).\end{aligned} \tag{8}$$

2.2. The approach incorporating a constitutive law with embedded discontinuity (CLED)

Averaging the velocity gradient (4) over a reference volume Δv, which includes the discontinuity interface, one obtains

$$\begin{aligned}&\frac{1}{\Delta v}\int_{\Delta v}\nabla^s\mathbf{v}\,dv\\ &= \frac{1}{\Delta v}\left(\int_{\Delta v}\nabla^s\hat{\mathbf{v}}\,dv + \int_{\Delta v}\mathcal{H}_{\Gamma_d}\nabla^s\tilde{\mathbf{v}}\,dv\right.\\ &\quad\left.+\int_{\Delta v}\delta_{\Gamma_d}(\hbar\tilde{\mathbf{v}}\otimes\mathbf{n})^s\,dv\right)\\ &= \frac{1}{\Delta v}\left(\int_{\Delta v}\nabla^s\hat{\mathbf{v}}\,dv + \int_{\Delta v}\mathcal{H}_{\Gamma_d}\nabla^s\tilde{\mathbf{v}}\,dv\right.\\ &\quad\left.+\int_{\Delta a}(\hbar\tilde{\mathbf{v}}\otimes\mathbf{n})^s\,da\right)\end{aligned} \tag{9}$$

where Δa is the area of the discontinuity surface within the reference volume. Assuming that the variations of the integrands in (9) are small, one has

$$\nabla^s\mathbf{v} = \nabla^s\hat{\mathbf{v}} + \frac{\Delta v^+ - \Delta v^-}{\Delta v}\nabla^s\tilde{\mathbf{v}} + \frac{\Delta a}{\Delta v}(\hbar\tilde{\mathbf{v}}\otimes\mathbf{n})^s. \tag{10}$$

Defining now $\chi = \Delta a/\Delta v$ and $\kappa = (\Delta v^+ - \Delta v^-)/(\hbar\,\Delta v)$, and using $\dot{\mathbf{g}} = \hbar\tilde{\mathbf{v}}$ one obtains

$$\begin{aligned}&\dot{\boldsymbol{\varepsilon}} = \nabla^s\mathbf{v}\\ \dot{\boldsymbol{\varepsilon}} = \dot{\hat{\boldsymbol{\varepsilon}}} + \dot{\tilde{\boldsymbol{\varepsilon}}} \quad &\text{where } \dot{\tilde{\boldsymbol{\varepsilon}}} = \nabla^s(\hat{\mathbf{v}} + \kappa\dot{\mathbf{g}})\\ &\dot{\tilde{\boldsymbol{\varepsilon}}} = \chi\,(\dot{\mathbf{g}}\otimes\mathbf{n})^s.\end{aligned} \tag{11}$$

In Eq. (11), $\dot{\hat{\boldsymbol{\varepsilon}}}$ represents the deformation in the intact material while $\dot{\tilde{\boldsymbol{\varepsilon}}}$ is the strain rate due to discontinuous motion along the interface averaged over the reference volume. In general, $\dot{\hat{\boldsymbol{\varepsilon}}}$ may include both elastic and plastic deformations in the intact material. Note that the representation (11) may be simplified by assuming that the discontinuity divides the element into two approximately equal volumes, in which case κ approaches zero, i.e. $\kappa \to 0$. It should be pointed out that the definition of the *characteristic dimension* $\chi = \Delta a/\Delta v$ employed in the current methodology is markedly different from that used in the strong discontinuity approach [26]. In the latter case, χ is defined as $1/h$, where h is effective bandwidth of the discontinuity.

Using now the additivity postulate and following the standard plasticity procedure, the stress rate in the intact material $\dot{\boldsymbol{\sigma}}_\Omega$ can be defined as,

$$\dot{\boldsymbol{\sigma}}_\Omega = \mathbb{D} : \dot{\hat{\boldsymbol{\varepsilon}}} = \mathbb{D} : (\dot{\boldsymbol{\varepsilon}} - \dot{\tilde{\boldsymbol{\varepsilon}}}) \tag{12}$$

where $\mathbb{D}$ is the fourth order stiffness operator. The traction vector across the interface must remain continuous, i.e. $\mathbf{n}\cdot\boldsymbol{\sigma}_\Omega = \mathbf{n}\cdot\boldsymbol{\sigma}_\Gamma$. Thus, imposing this constraint and writing the constitutive relation for the interfacial material in the rate form as $\dot{\boldsymbol{\sigma}}_\Gamma\cdot\mathbf{n} = \dot{\mathbf{t}} = \mathbf{K}\cdot\dot{\mathbf{g}}$, one obtains,

$$\mathbf{n}\cdot\mathbb{D} : \dot{\tilde{\boldsymbol{\varepsilon}}} = \mathbf{K}\cdot\dot{\mathbf{g}} \quad \text{where } \mathbf{K} = \mathbf{R}\cdot\mathbf{K}^*\cdot\mathbf{R}^T. \tag{13}$$

In Eq. (13), $\mathbf{K}$ is the tangential stiffness operator for the interfacial material in the global coordinate system while $\mathbf{K}^*$ defines the same operator related to the local coordinate system along the interface. Using Eq. (13), together with Eqs. (11) and (12), one obtains

$$\begin{aligned}&\dot{\tilde{\boldsymbol{\varepsilon}}} = \mathbb{E} :: \mathbb{D} : \dot{\boldsymbol{\varepsilon}}\\ &\text{where } \mathbb{E} = \chi\,\mathbf{n}\otimes(\mathbf{K} + \chi\,\mathbf{n}\cdot\mathbb{D}\cdot\mathbf{n})^{-1}\otimes\mathbf{n}.\end{aligned} \tag{14}$$

Now, substituting Eq. (14) into the constitutive relation (12) yields

$$\dot{\boldsymbol{\sigma}}_\Omega = \tilde{\mathbb{D}} : \dot{\boldsymbol{\varepsilon}} \quad \text{where } \tilde{\mathbb{D}} = \mathbb{D} - \mathbb{D} : \mathbb{E} : \mathbb{D}. \tag{15}$$

Note that using matrix notation, relations (11), (14) and (15) can be expressed as

$$\begin{aligned}&\{\dot{\boldsymbol{\varepsilon}}\} = [\mathbf{L}]\{\mathbf{v}\}\\ \{\dot{\boldsymbol{\varepsilon}}\} = \{\dot{\hat{\boldsymbol{\varepsilon}}}\} + \{\dot{\tilde{\boldsymbol{\varepsilon}}}\} \quad &\text{where } \{\dot{\tilde{\boldsymbol{\varepsilon}}}\} = [\mathbf{L}]\{\hat{\mathbf{v}} + \kappa\,\dot{\mathbf{g}}\}\\ &\{\dot{\tilde{\boldsymbol{\varepsilon}}}\} = \chi\,[\mathbf{n}]\{\dot{\mathbf{g}}\}\\ \{\dot{\tilde{\boldsymbol{\varepsilon}}}\} = [\mathbb{E}][\mathbb{D}]\{\dot{\boldsymbol{\varepsilon}}\} \quad &\text{where } [\mathbb{E}] = \chi\,[\mathbf{n}]\left[\bar{\mathbf{K}}\right]^{-1}[\mathbf{n}]^T\\ &\left[\bar{\mathbf{K}}\right] = [\mathbf{K}] + \chi\,[\mathbf{n}]^T[\mathbb{D}][\mathbf{n}]\\ \{\dot{\boldsymbol{\sigma}}_\Omega\} = [\mathbb{D}_T]\{\dot{\boldsymbol{\varepsilon}}\} \quad &\text{where } [\mathbb{D}_T] = [\mathbb{D}] - [\mathbb{D}][\mathbb{E}][\mathbb{D}]\end{aligned} \tag{16}$$

where, $\left\{\nabla^s \bullet\right\} = [\mathbf{L}]\{\bullet\}$ and

$$[\mathbf{n}] = \begin{bmatrix} n_1 & 0 & 0 \\ 0 & n_2 & 0 \\ 0 & 0 & n_3 \\ n_2 & n_1 & 0 \\ n_3 & 0 & n_1 \\ 0 & n_3 & n_2 \end{bmatrix}; \quad [\mathbf{L}] = \begin{bmatrix} \frac{\partial}{\partial x} & 0 & 0 \\ 0 & \frac{\partial}{\partial y} & 0 \\ 0 & 0 & \frac{\partial}{\partial z} \\ \frac{\partial}{\partial y} & \frac{\partial}{\partial x} & 0 \\ \frac{\partial}{\partial z} & 0 & \frac{\partial}{\partial x} \\ 0 & \frac{\partial}{\partial z} & \frac{\partial}{\partial y} \end{bmatrix}. \tag{17}$$

Thus, in the context of CLED, for elements experiencing cracking, the constitutive relation (15) must be employed.

2.3. Application of CLED to modeling of flow problems in the presence of discontinuities: Fourier/Darcy law with embedded discontinuity

Noting the conceptual similarities between a discrete representation of FEM/CLED and XFEM, one can use the former approach to deal with virtually any type of discontinuities that can be addressed through XFEM approach. One example, which is described here, is the application to modeling discontinuities in scalar field problems such as heat and fluid flow.

The discontinuous scalar field variable φ can be expressed as

$$\varphi = \hat{\varphi} + \mathcal{H}\tilde{\varphi} \rightarrow \nabla\varphi = \nabla\hat{\varphi} + \mathcal{H}\nabla\tilde{\varphi} + \delta_\Gamma \tilde{\varphi}\mathbf{n} \tag{18}$$

where $\hat{\varphi}$ and $\tilde{\varphi}$ are continuous functions and $\mathcal{H} = \mathcal{H}(\phi)$ is the Heaviside function, as defined in (1). Averaging Eq. (11) over a small enough reference volume, and following the approach described in the previous section, one can obtain

$$\nabla\varphi \approx \nabla\hat{\varphi} + \chi\,\tilde{\varphi}\mathbf{n} \tag{19}$$

as an approximation of the discontinuous field. The parameter χ depends on the geometry of the discontinuity within the referential volume, and its definition is analogous to that given earlier. By invoking representation (18), the Fourier law can now be rephrased to define the flow within a domain containing a discontinuity, i.e.

$$\mathbf{q} = -\mathbf{k}\cdot\nabla\hat{\varphi} = -\mathbf{k}\cdot\nabla\varphi + \chi\mathbf{k}\cdot\,\tilde{\varphi}\mathbf{n}. \tag{20}$$

Here, $\mathbf{q}$ is the flux vector, and $\mathbf{k}$ as either the thermal or hydraulic conductivity operator for heat transfer or fluid flow in porous media, respectively. The above representation can be applied within the context of any given interfacial properties. Here, the simple case of thermally isolated/impervious interfaces is addressed, for which $q_n = \mathbf{n}\cdot\mathbf{q} = 0$ on Γ_d. Imposing this constraint in Eq. (20), yields

$$-\mathbf{n}\cdot\mathbf{k}\cdot\nabla\varphi + \chi\tilde{\varphi}\,\mathbf{n}\cdot\,\mathbf{k}\cdot\mathbf{n} = 0$$
$$\rightarrow \tilde{\varphi} = \frac{1}{\chi k_{nn}}\mathbf{n}\cdot\mathbf{k}\cdot\nabla\varphi \tag{21}$$

where $k_{nn} = \mathbf{n}\cdot\,\mathbf{k}\,\cdot\mathbf{n}$. Substituting Eq. (21) back into Eq. (20), the *Fourier law with embedded discontinuity* can be expressed as

$$\mathbf{q} = -\tilde{\mathbf{k}}\cdot\nabla\varphi \quad \text{where } \tilde{\mathbf{k}} = \mathbf{k} - \frac{(\mathbf{k}\cdot\mathbf{n})\otimes(\mathbf{n}\cdot\mathbf{k})}{k_{nn}}. \tag{22}$$

Note that $\tilde{\mathbf{k}}$ which is an equivalent thermal/hydraulic conductivity operator for a region which contains a thermally non-conductive/impervious crack, is now independent of χ. This allows for a simple and straightforward implementation of this approach in standard numerical codes.

3. Discrete crack propagation

As shown in several studies addressing discrete modeling of crack [14,23], the path of crack propagation can be traced by the level-set method. Based on this approach, a moving/propagating interface $\Gamma_d(t)$ can be defined as the zero level set of a function $\phi(\mathbf{x}, t)$, i.e., $\Gamma_d(t) = \{\mathbf{x}|\phi(\mathbf{x}, t) = 0\}$.
The function $\phi(\mathbf{x})$ itself can be expressed as the signed distance function

$$\phi(\mathbf{x}) = \text{sign}\,\{\mathbf{n}_\Gamma\cdot(\mathbf{x}-\mathbf{x}_\Gamma)\}\ \min\|\mathbf{x}-\mathbf{x}_\Gamma\| \tag{23}$$

where $\mathbf{n}_\Gamma$ is a normal to the direction of propagation, $\mathbf{x}$ is an arbitrary point in Ω, and $\mathbf{x}_\Gamma$ is the point located on the interface at the minimum distance from $\mathbf{x}$.

For two dimensional XFEM simulations, as performed in this study, the interface is defined as a polygon of line segments passing through elements in which a crack has formed. Hence, for a node that is common for two adjacent enriched elements, the level set function can be defined as the minimum distance from this node to the respective line segments associated with these elements. For each element, the values of the level-set function at Gauss points can be determined from nodal values using FEM interpolation functions, i.e. $\phi = \sum N_i\bar{\phi}_i$.

In the case of CLED, i.e. the framework incorporating a constitutive law with embedded discontinuity, the same approach is used for tracing the propagating crack. Thus, by analogy to XFEM, the crack is introduced at the element level and the characteristic dimension χ is evaluated based on the volume of the element and the geometry of the propagating crack. Consequently, at all Gauss points associated with this element the constitutive relation (15) that employs the volume averaging is used. Given the similarity of this procedure to the general methodology for tracing the interface adopted in XFEM, the results obtained from these two approaches are very similar. Further details regarding the specification of the orientation of the propagating path are provided in [1]. The main steps of this approach are summarized in the flow chart in Fig. 1.

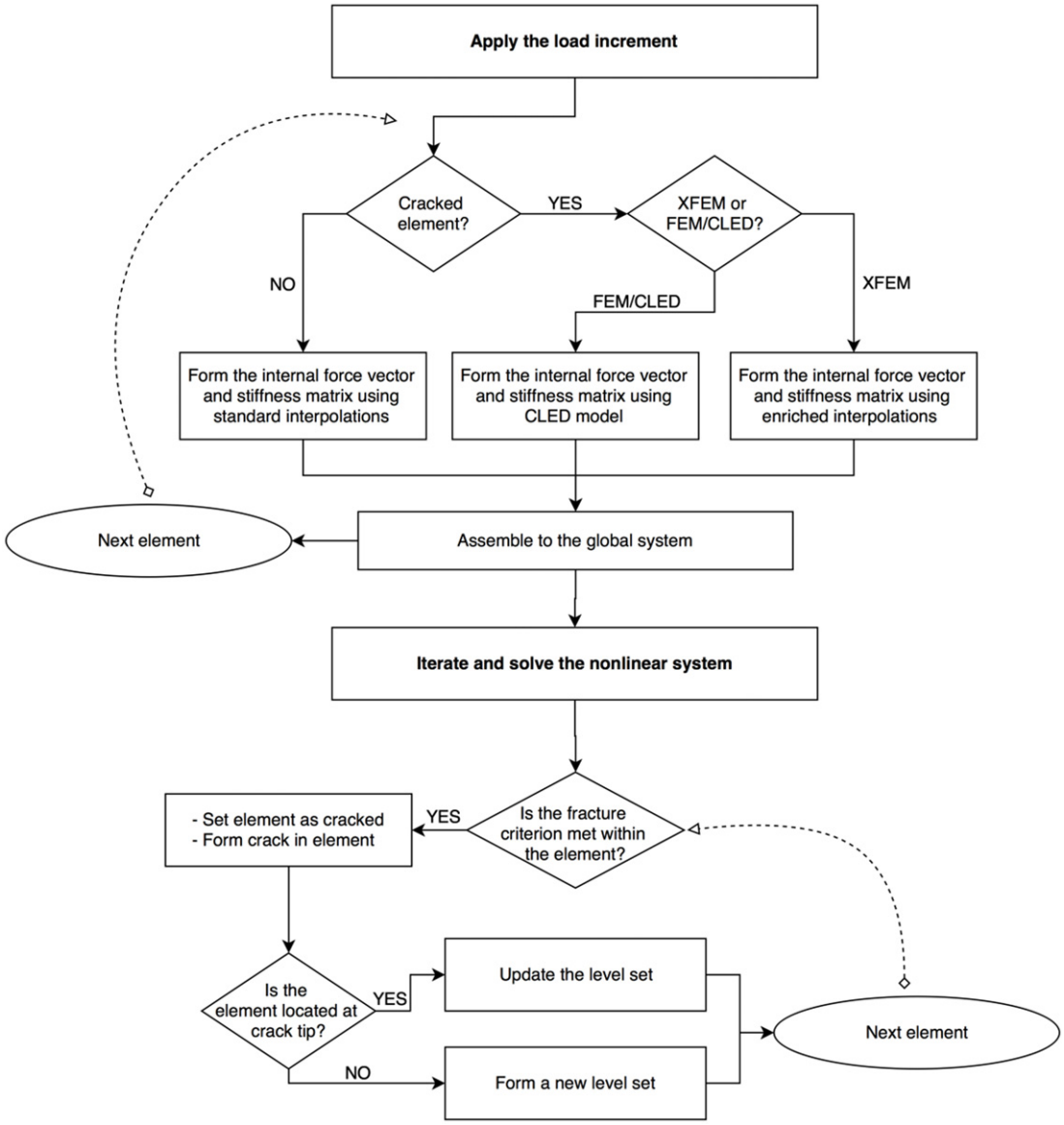

Fig. 1. Flow chart defining the crack propagation strategy for both FEM/CLED and XFEM formulations.

4. Numerical simulations for a traction free crack

In this section, the problem of traction free cracks is investigated using the formulation introduced in the previous section. Two cases are considered involving an edge crack and a crack located inside the considered domain. The energy release rate is used as a deterministic way of comparing the results with both XFEM (without tip enrichment) and an analytical solution.

For the case of FEM/CLED, imposing the traction free condition results in a simple procedure that can be easily incorporated within any FEM code. In order to impose this constraint, one can set $\dot{\mathbf{t}} = \mathbf{0}$ or equivalently $\mathbf{K} = \mathbf{0}$ in Eq. (14). The stiffness operator $\tilde{\mathbb{D}}$ will then reduce to

$$\tilde{\mathbb{D}} = \mathbb{D} - \mathbb{D} : \mathbb{E} : \mathbb{D}$$
$$\text{where } \mathbb{E} = \mathbf{n} \otimes (\mathbf{n} \cdot \mathbb{D} \cdot \mathbf{n})^{-1} \otimes \mathbf{n} \tag{24}$$

which is independent of the characteristic dimension χ. Eq. (24) can be conveniently defined in the local coordinate system attached to the crack. The matrix form of the operator $\tilde{\mathbf{n}}$, Eq. (16), can then be expressed as

$$[\tilde{\mathbf{n}}] = \begin{bmatrix} \tilde{n}_1 & 0 & 0 \\ 0 & \tilde{n}_2 & 0 \\ 0 & 0 & \tilde{n}_3 \\ \tilde{n}_2 & \tilde{n}_1 & 0 \\ \tilde{n}_3 & 0 & \tilde{n}_1 \\ 0 & \tilde{n}_3 & \tilde{n}_2 \end{bmatrix} = \begin{bmatrix} 1 & 0 & 0 \\ 0 & 0 & 0 \\ 0 & 0 & 0 \\ 0 & 1 & 0 \\ 0 & 0 & 1 \\ 0 & 0 & 0 \end{bmatrix}. \tag{25}$$

Thus, representation (24) can be written in a component form as

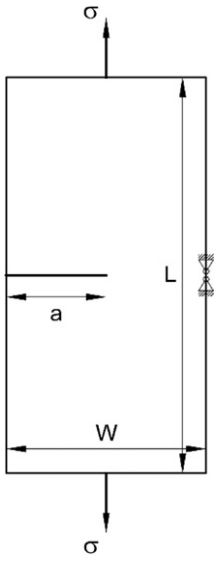

Fig. 2. Edge crack problem.

$$[\tilde{\mathbb{D}}] = \begin{bmatrix} 0 & 0 & 0 & 0 & 0 & 0 \\ 0 & \tilde{D}_{22} & \tilde{D}_{23} & 0 & 0 & 0 \\ 0 & \tilde{D}_{23} & \tilde{D}_{22} & 0 & 0 & 0 \\ 0 & 0 & 0 & 0 & 0 & 0 \\ 0 & 0 & 0 & 0 & 0 & 0 \\ 0 & 0 & 0 & 0 & 0 & G \end{bmatrix}$$

$$\text{where} \quad \begin{aligned} \tilde{D}_{22} &= -\frac{D_{12}^2}{D_{11}} + D_{11} = -\frac{\lambda^2}{\lambda + 2\mu} + \lambda + 2\mu \\ \tilde{D}_{23} &= -\frac{D_{12}^2}{D_{11}} + D_{12} = -\frac{\lambda^2}{\lambda + 2\mu} + \lambda \end{aligned} \tag{26}$$

where λ and μ are Lame constants. This simple local representation of $\tilde{\mathbb{D}}$ is an efficient way of employing the CLED approach for modeling of traction free cracks with predefined dimensions. In this case, since the orientation of the crack is known in advance, the discontinuous tangential operator can be defined through Eq. (26) prior to the analysis. This operator is similar to an anisotropic elastic matrix, which can be defined in most FEM packages.

4.1. Mode I edge crack problem

The first problem that is investigated is the two-dimensional plane stress Mode I edge crack under tensile stress. The problem geometry is based on the study reported in [12], and it is shown in Fig. 2.

The tensile traction $\sigma = 1$ psi is applied at both the top and the bottom surfaces, while two points on the right side are constrained to ensure the stability. The FE discretizations employed in this analysis are shown in Fig. 3. For the case of edge crack the analytical value of stress intensity factor K_I is [27]

$$\begin{aligned} K_I &= C\sigma\sqrt{\pi a}, \\ C &= 1.12 - 0.231\left(\frac{a}{w}\right) + 10.55\left(\frac{a}{w}\right)^2 \\ &\quad - 21.72\left(\frac{a}{w}\right)^3 + 30.39\left(\frac{a}{w}\right)^4 \end{aligned} \tag{27}$$

with $K_{II} = 0$. The energy release rate can then be calculated analytically from J Integral-stress intensity factor relation

$$J = \frac{K_I^2 + K_{II}^2}{E'}$$

$$\text{with } E' = \begin{cases} E & \text{Plane Stress} \\ E/(1-\nu^2) & \text{Plane Strain.} \end{cases} \tag{28}$$

Two approaches are used here, i.e. CLED with the constitutive equation (26) assigned to the elements containing a crack, and XFEM analysis without the tip enrichments. The J-Integral calculations, using average of 5 contours, are shown in Table 1.

It is evident here that both CLED and XFEM without tip enrichment give results with a very similar accuracy, except for the second type of discretization. In the latter case, the interface passes very close to the nodes embedded in the FE mesh. As a result, the Jacobian operator in XFEM formulation becomes ill-conditioned as the volume on one side of partitioned element is almost zero. There have been various special techniques suggested in the literature to resolve this issue (e.g., abandoning integration over the negligible volume, correcting the interface orientation,

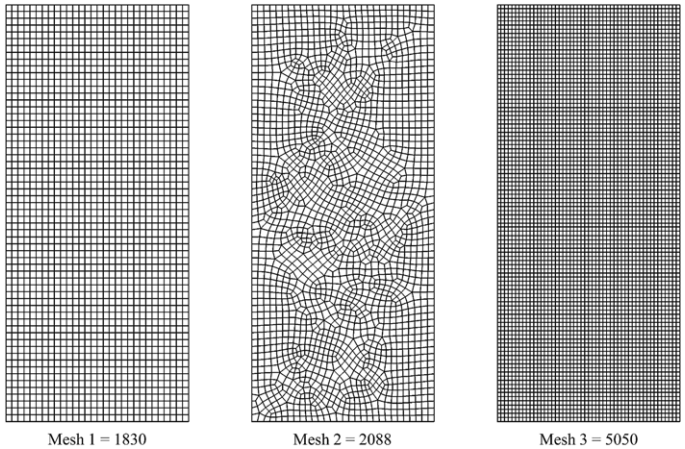

Fig. 3. Different discretizations used in numerical simulations.

Table 1
Relative error of J-Integral calculations from FEM/CLED and XFEM w.r.t. analytical solution for the edge crack problem.

	Analytical	FEM/CLED	RE	XFEM	RE
Mesh 1	8.78E−04	1.07E−03	21.7	1.07E−03	21.4
Mesh 2	8.78E−04	9.08E−04	3.4	1.00E−05	98.9
Mesh 3	8.78E−04	1.08E−03	22.7	1.07E−03	22.2

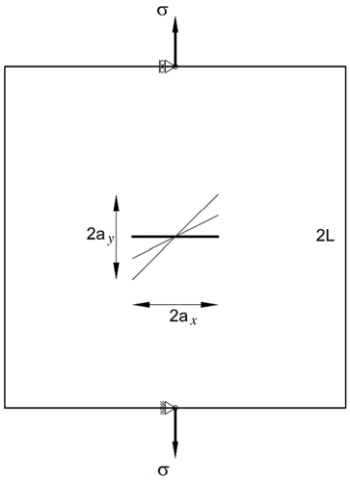

Fig. 4. Center crack problem.

etc.), however, the results reported here are based on the original approach that employs the integration scheme with the back triangulation. It should be noted that this problem does not arise within the discrete FEM/CLED formulation as the constitutive relation is integrated over the entire element resulting in less relative error.

It is apparent from Table 1 that although both approaches yield very similar results, the relative errors with respect to the analytical solution are, in general, rather significant. The reason lies in the inability of standard FEM interpolations to reproduce crack tip singularities. In XFEM, this can be resolved by enriching the tip element with singular asymptotic functions, as suggested in various publications [12,14,28]. Note that the local tip enrichment can also be applied to FEM/CLED approach. In this case, the only part of the domain that requires the enrichment would be the tip element. In most of the practical applications of XFEM the tip enrichments are ignored, which makes the CLED approach very attractive in view of its simplicity and comparable accuracy.

4.2. Center crack problem

The second problem analyzed here is that involving a crack in the center of a square plate, loaded under plane stress condition. The geometry of the problem is shown in Fig. 4.

In this case, three different orientations of the crack are considered, i.e. a_x fixed with $a_x = 0.1$ m and a_y varying with $a_y = (0,\ 0.05,\ 0.1)$ m respectively. The plate is subjected to boundary traction $\sigma = 100$ MPa applied at the top and the bottom faces. The center node at the bottom is fixed while the center node on top is horizontally constrained to provide stability. The material/geometric properties are

$$E = 200\ \text{GPa}, \qquad \upsilon = 0.3, \qquad L = 1.0\ \text{m}.$$

Three different meshes are again used for this study, as shown in Fig. 5, while the analytical solution for a center crack within an infinite plate is [12]

$$K_I = \sigma\sqrt{\pi a}\cos^2\beta, \qquad K_{II} = \sigma\sqrt{\pi a}\sin\beta\cos\beta. \tag{29}$$

For the case of horizontal crack with $a_y = 0$ m, the results of J-Integral calculations are provided in Table 2. For an inclined crack, the calculation were performed using the third mesh only and the corresponding results are provided in Table 3.

Again, it is evident from Tables 2 and 3 that the results of FEM/CLED and XFEM calculations are very close. For the case of inclined crack with $a_y = 0.05$ m, the estimate from FEM/CLED has less relative error as compared to XFEM approach.

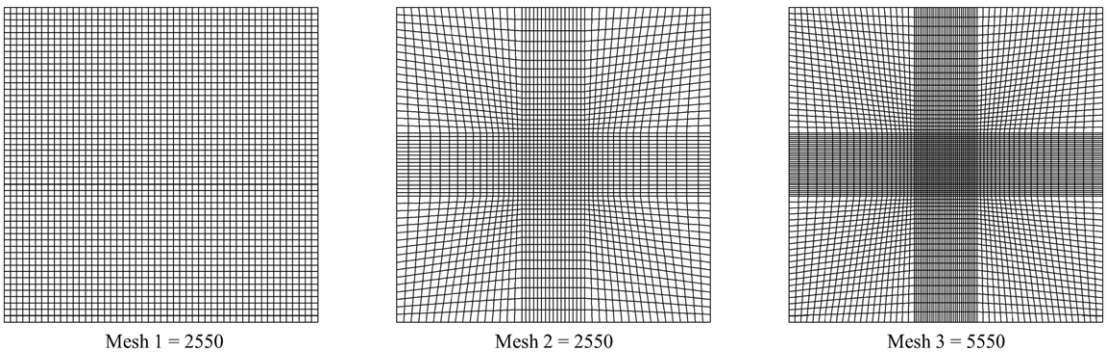

Fig. 5. The discretizations that are used for analysis.

Table 2
Relative error of J-Integral calculations from FEM/CLED and XFEM w.r.t. analytical solution for horizontal crack.

	Analytical	FEM/CLED	RE	XFEM	RE
Mesh 1	1.57E+04	2.05E+04	30.3	2.02E+04	28.9
Mesh 2	1.57E+04	2.03E+04	29.5	2.02E+04	28.7
Mesh 3	1.57E+04	1.91E+04	21.4	1.90E+04	20.9

Table 3
Relative error of J-Integral calculations from FEM/CLED and XFEM w.r.t. analytical solution for inclined cracks with Mesh 3.

	Analytical	FEM/CLED	RE	XFEM	RE
$a_y = 0.0$ m	1.57E+04	1.91E+04	21.4	1.90E+04	20.9
$a_y = 0.05$ m	1.40E+04	1.41E+04	0.2	1.68E+04	19.8
$a_y = 0.1$ m	1.11E+04	8.69E+03	21.7	1.35E+04	21.4

5. Numerical simulations of cohesive crack propagation

In this section, the problem of a cohesive crack propagation is investigated using FEM/CLED and the results are compared with XFEM. In order to describe the mechanical characteristics of the interfacial material, a simple damage model, similar to that proposed in Ref. [15], is employed. Within this framework, an exponential relation for the evolution of cohesive forces acting on the crack faces is assumed, i.e.

$$\mathcal{F}_t(g_n) = \begin{cases} F_t & g_n \le \delta_c \\ F_t e^{\frac{-F_t}{G_f}(g_n - \delta_c)} & g_n > \delta_c \end{cases} \tag{30}$$

where, δ_c is the critical separation for imposing the contact condition in a penalty approach, F_t is the initial tensile strength of the material, and $\mathcal{F}_t(g_n)$ is the tensile strength at separation g_n. The failure criterion is written as

$$f(t_n, g_n) = t_n - \mathcal{F}_t(g_n). \tag{31}$$

During an active loading process, there is $f(t_n, g_n) = 0$, so that the normal traction t_n can be expressed as

$$t_n = F_t \exp\left(-\frac{F_t}{G_f}(g_n - \delta_c)\right). \tag{32}$$

The shear traction t_t can be defined in terms of discontinuity in the tangential component of displacement g_t

$$t_t = d\,K_t g_t = \frac{\mathcal{F}_t}{F_t} K_t g_t \tag{33}$$

where $d = \mathcal{F}_t/F_t$ is the damage parameter and K_t is the shear stiffness of the interfacial material. Referring the problem to the local coordinate system along the crack, the incremental form of Eqs. (32) and (33) can be written as

$$\begin{aligned} \dot{t}_n &= k_{11}\dot{g}_n = \left\{-\frac{F_t^2}{G_f}\exp\left(-\frac{F_t}{G_f}(g_n - \delta_c)\right)\right\}\dot{g}_n \\ \dot{t}_{t_i} &= k_{i1}\dot{g}_n + k_{i2}\dot{g}_{t_i} \\ &= \left\{-\frac{F_t}{G_f}\exp\left(-\frac{F_t}{G_f}(g_n - \delta_c)\right) K_t g_{t_i}\right\}\dot{g}_n \\ &\quad + \{d\,K_t\}\dot{g}_{t_i}, \quad i = 1, 2 \end{aligned} \tag{34}$$

where the indexes 1, 2 define the in-plane orientations. Thus, the constitutive relation for the interfacial material can be expressed in the rate form

$$\dot{\mathbf{t}}^* = \mathbf{K}^* \cdot \dot{\mathbf{g}}^* \quad \text{where } \mathbf{K}^* = \begin{bmatrix} k_{11} & 0 & 0 \\ k_{21} & k_{22} & 0 \\ k_{31} & 0 & k_{33} \end{bmatrix} \tag{35}$$

where $\mathbf{K}^*$ is the tangential stiffness operator.

5.1. Three point bending problem

The first example given here involves a simply supported concrete beam subjected to an increasing vertical displacement applied in the middle of the span, Fig. 6. The geometry is taken from the Ref. [16]. The beam has dimensions $l = 600$ mm and $b = t = 150$ mm, where t is the out of plane thickness, and the material properties are as follows

$E = 36.5 \times 10^3$ MPa; $\quad \upsilon = 0.1$;
$F_t = 3.19$ MPa; $\quad G_f = 0.05$ N/mm;
$\delta_c = 1 \times 10^{-4}$ mm.

The key results of the analysis are presented in Figs. 7–9. Fig. 7 shows the damage pattern that is superimposed on the distribution of σ_{11}. The solution is identical here for both XFEM and FEM/CLED simulations. The failure process involves development of tensile cracks near the middle of the span and subsequent propagation of a dominant vertical crack in the center of the beam. These results are now compared in Fig. 8 with the solution using the original *smeared* cracking approach, i.e. CLED without the enhancement for discrete representation of crack path. The load–displacement (δ) response is shown in Fig. 9. The behavior becomes unstable after reaching the peak (see the figure on the left-hand side). It is evident that the solution based on the enhanced FEM/CLED is virtually identical

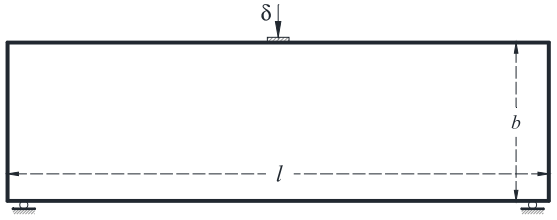

Fig. 6. Three point bending test on a concrete beam ($l = 4b = 4t = 600$ mm).

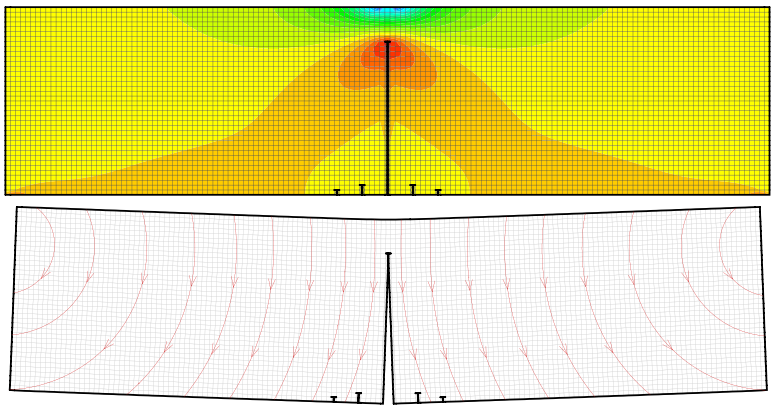

Fig. 7. Top: Cracking pattern depicted on σ_{11} contour for XFEM or FEM/CLED analysis (identical solutions); Bottom: Cracking pattern and deformation vector plotted on the deformed shape (Scale = 100).

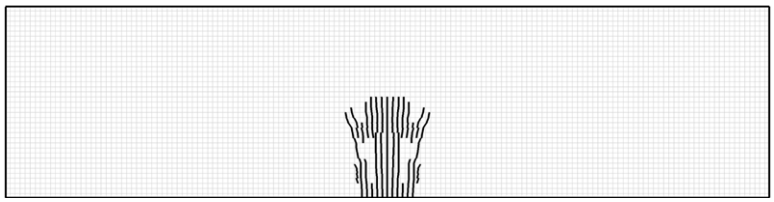

Fig. 8. The crack pattern obtained using the classical smeared FEM/CLED approach.

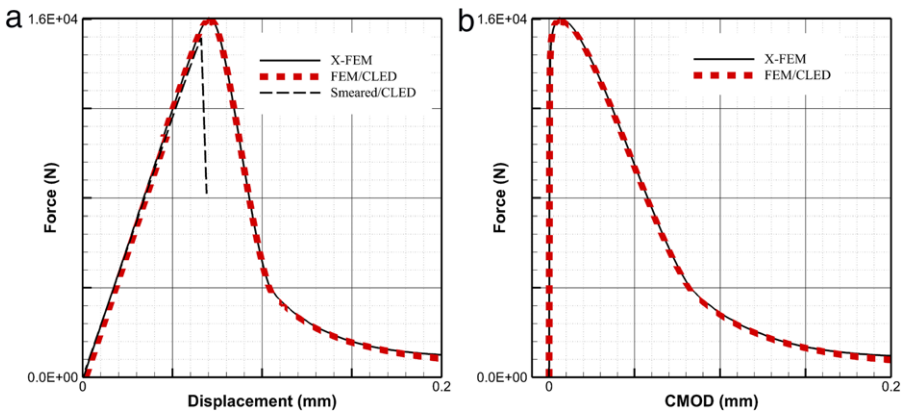

Fig. 9. Reaction force vs. (a) vertical displacement and (b) crack mouth opening displacement (CMOD).

to that obtained using XFEM methodology, while there is a markable difference in the results of CLED approach corresponding to discrete and smeared cracking.

5.2. Nooru-Mohamed mixed mode cracking test

The second problem that is studied here is based on the experimental test performed by Nooru-Mohamed [29] and involves a mixed mode cracking. The geometry of the problem is shown in Fig. 10. The specimen has the dimensions of $l = b = 200$ mm, $c = 25$ mm, and out of plane thickness $t = 50$ mm. Material properties, are as reported in [29], i.e.

$E = 29 \times 10^3$ MPa; $\nu = 0.15$;

$F_t = 3.67$ MPa; $G_f = 0.05$ N/mm;

$\delta_c = 1 \times 10^{-3}$ mm.

The loading process consists of two different stages. First, a horizontal displacement of $\delta_x = 0.005$ mm is applied along the vertical faces under $\delta_y = 0$. At this stage, referred to as the shearing stage, no cracks are formed. Then, a vertical displacement δ_y is imposed along the horizontal faces, while the δ_x remains constant. This stage results in onset and propagation of tensile cracks. The response of the structure is shown Figs. 11–14.

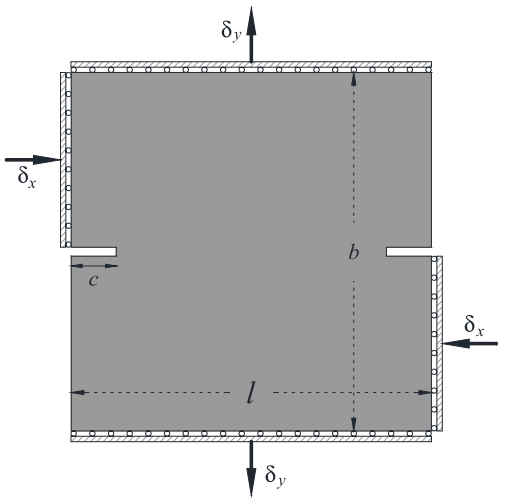

Fig. 10. Mixed mode cracking test ($l = b = 200$ and $c = 25$ mm).

Fig. 11 shows the cracking pattern superimposed on the contours of horizontal and vertical displacements, while Fig. 12 gives a similar representation in terms of displacement vectors. In this case, two macrocracks form, at the notches, and propagate towards the center of the specimen. The fracture pattern is consistent with the experimental evidence [29] and it is identical for both XFEM and FEM/CLED approaches.

Figs. 13–14 present the evolution of the components of the reaction force against imposed boundary displacements as well as the crack tip opening. Again, as the vertical displacement is imposed, the response becomes unstable. The global characteristics are very similar for both methodologies, i.e. XFEM and FEM/CLED. This is particularly evident both prior to as well as at the early stages of the onset of global instability, which is of primary interest for practical engineering purposes. At very advanced stages of deformation, the enhanced volume averaging method predicts less crack opening than the XFEM.

6. Modeling of heat transfer around thermally isolated crack

The last numerical study presented here deals with application of the Fourier law with embedded discontinuity, as discussed in Section 2.3. In this case, the equivalent thermal conductivity operator $\tilde{\mathbf{k}}$ for elements that contain a thermally non-conductive crack is defined by Eq. (22). Referring the problem to the local coordinate system along the crack of unit normal $\tilde{n}_i = (1, 0, 0)$ and assuming that

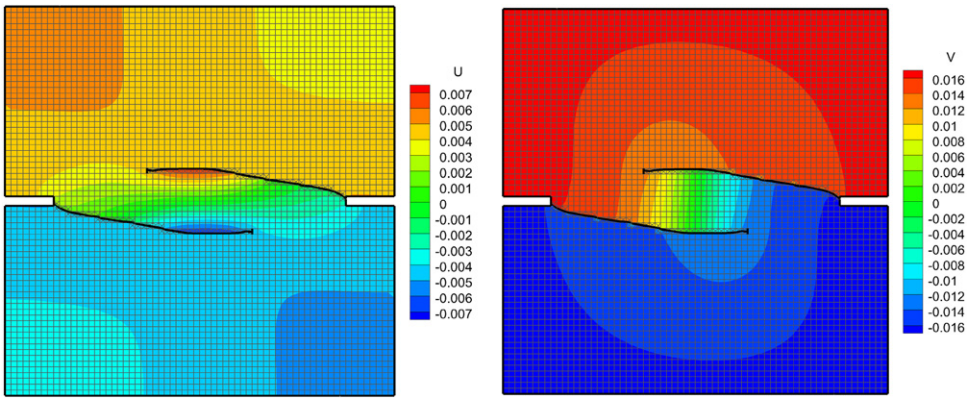

Fig. 11. Cracking pattern superimposed on the contours of horizontal (u) and vertical (v) displacements (mm).

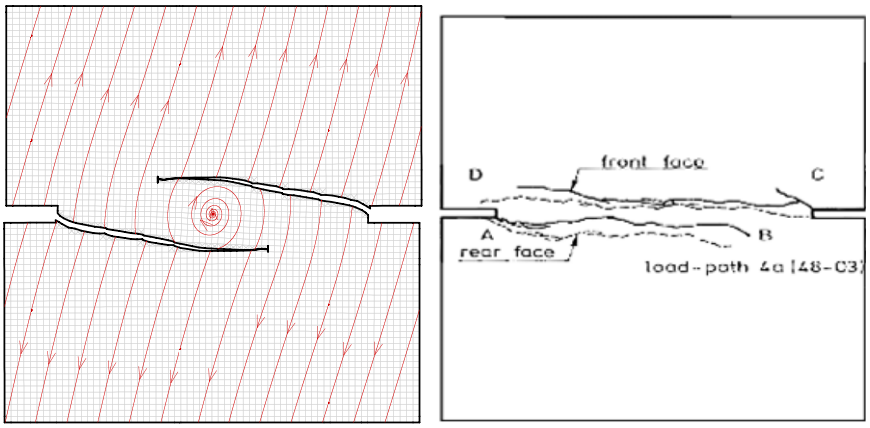

Fig. 12. Left: Cracking pattern and the displacement vector plotted on the deformed shape (scale factor = 100); Right: Experimental results [29].

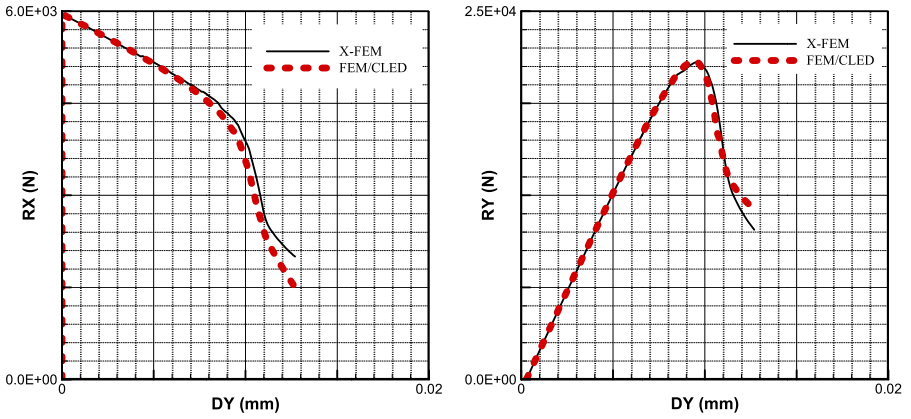

Fig. 13. Reaction components (RX and RY) vs. vertical displacement (DY).

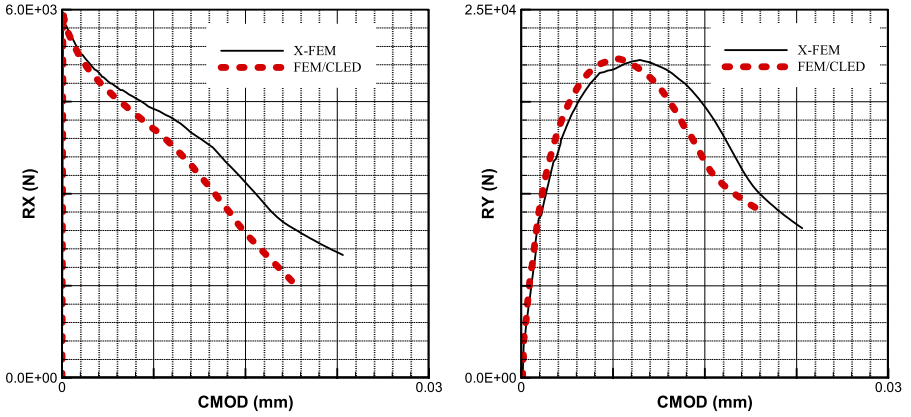

Fig. 14. Reaction force vs. CMOD (crack mouth opening displacement).

the intact material is isotropic, the expression for $\tilde{\mathbf{k}}$ reduces to a simple form

$$\tilde{\mathbf{k}} = \begin{bmatrix} 0 & 0 & 0 \\ 0 & k & 0 \\ 0 & 0 & k \end{bmatrix} \tag{36}$$

where k is the conductivity of the intact material. It is evident that the representation (36) can be easily incorporated in any standard FEM package through an option of material anisotropy.

The illustrative example provided here is similar to that reported in [16] and concerns a steady-state heat flow within the domain containing thermally isolated cracks. Three different scenarios are examined, viz. a single horizontal crack with $\beta = 0^\circ$, an inclined one with $\beta = 45^\circ$, and a set of nine randomly distributed cracks. The geometry of the problem is shown in Fig. 15. The analysis is conducted here with $(L, \mathrm{a}) = (1, 0.25)$ m for a single crack and $(L, \mathrm{a}) = (1, 0.1)$ m for multiple cracks, while the assumed temperature gradient is $\theta_{top} - \theta_{bot} = +20$ K. The coefficient of thermal conductivity k is taken as $k = 1$ W/mK.

The main results are shown in Figs. 16–17 and are presented in terms of stream lines which are superimposed on the temperature field normalized with respect to θ_{top}.

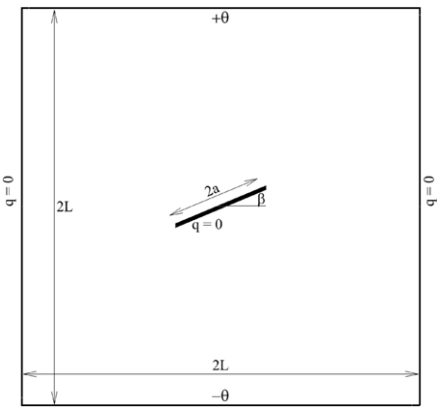

Fig. 15. Geometry of the problem for heat transfer around an insulated crack.

Fig. 16 gives the solution for a single crack, while Fig. 17 shows the heat flow pattern in the presence of randomly distributed cracks. It is evident that the simple model proposed here is capable of an adequate representation scalar field problems involving constrained discontinuities.

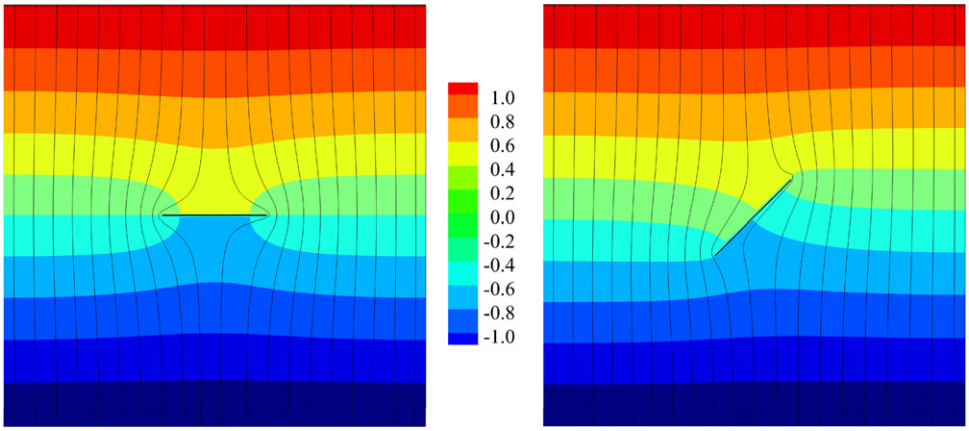

Fig. 16. Heat flux stream lines superimposed on the normalized temperature field.

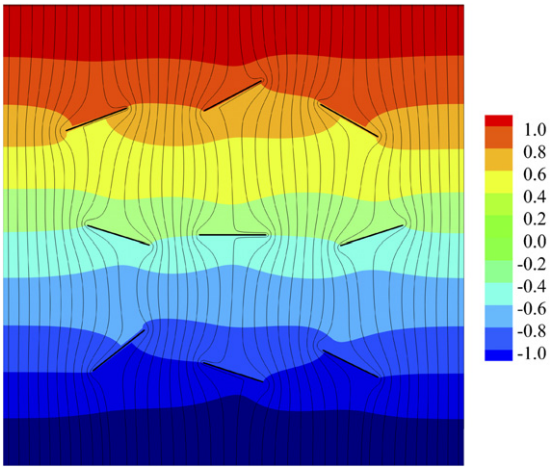

Fig. 17. Heat flux stream lines for the randomly distributed multiple cracks superimposed on the normalized temperature field.

7. Concluding remarks

The primary focus of the study presented here, which is an extension of a recently published work [1], was on application to analysis of fracture problems involving traction free and cohesive cracks. In addition, the flow problems in the presence of non-conductive discontinuities have been addressed by introducing a Fourier flow model with embedded discontinuity.

In the first part of this work, the issue of the accuracy of the solution based on FEM/CLED analysis of pre-existing cracks was addressed. The results were compared with XFEM approach without the tip enrichments. The reason for this choice was that in most engineering applications, especially those involving analysis of large scale structures, the use of tip enrichments is usually avoided. The comparison was based on the energy release rate (J-integral) calculations around the crack tip and the relative error was assessed in relation to the analytical solution. The comparison showed that both approaches, i.e. CLED and XFEM, give very similar results in terms of reproducing the displacement/stress fields around the crack. The comparison was conducted for an edge crack as well as center cracks of different orientations. It is noted that the CLED approach can also be used in conjunction with the tip enrichments to reproduce the tip singularities. In this case, the enrichment will only be required for the tip element.

In the second part of this work, the cohesive crack propagation problems have been addressed. Two sets of numerical simulations were conducted. In this first example, involving a three-point bending test, the discrete representation of CLED was compared with its original 'smeared' version as well as XFEM. It was demonstrated that the enhanced discrete representation can reproduce virtually identical solution to that of XFEM in terms of both the crack propagation mechanism and the stress/strain distribution. However, the 'smeared' representation provides a simplified picture of the fracture pattern and becomes numerically unstable after reaching the peak load. The second example, which involved a simulation of a mixed fracture mode, led to similar conclusions in terms of accuracy of CLED in relation to XFEM.

In the last part, a new representation of Fourier law was introduced that takes into account the discontinuity within the flux domain. The methodology was applied to the problem involving a steady state heat flow around non-conductive interfaces. Again, the procedure can be extended to take into account different thermal conductivities of cracks. This can be an attractive feature for problems such as hydraulic fracturing due to its efficiency and simplicity.

References

[1] E. Haghighat, S. Pietruszczak, On modeling of discrete propagation of localized damage in cohesive-frictional materials, Int. J. Numer. Anal. Methods Geomech. (2015) http://dx.doi.org/10.1002/nag.2368.
[2] D. Ngo, A.C. Scordelis, Finite element analysis of reinforced concrete beams, ACI J. Proc. 64 (1967).
[3] A.R. Ingraffea, V. Saouma, Numerical modeling of discrete crack propagation in reinforced and plain concrete, Fract. Mech. Concr. Struct. Appl. Numer. Calc. (1985) 171–225. Springer.
[4] D.M. Parks, The virtual crack extension method for nonlinear material behavior, Comput. Methods Appl. Mech. Engrg. 12 (1977) 353–364. http://dx.doi.org/10.1016/0045-7825(77)90023-8.
[5] J. Lubliner, J. Oliver, S. Oller, E. Oñate, A plastic-damage model for concrete, Internat. J. Solids Struct. 25 (1989) 299–326. http://dx.doi.org/10.1016/0020-7683(89)90050-4.

[6] J.G. Rots, J. Blaauwendraad, Crack models for concrete, discrete or smeared? Fixed, multi-directional or rotating? HERON 34 (1) (1989).
[7] S. Pietruszczak, Z. Mróz, Finite element analysis of deformation of strain-softening materials, Internat. J. Numer. Methods Engrg. 17 (1981) 327–334. http://dx.doi.org/10.1002/nme.1620170303.
[8] J.C. Simo, J. Oliver, F. Armero, An analysis of strong discontinuities induced by strain-softening in rate-independent inelastic solids, Comput. Mech. 12 (1993) 277–296. http://dx.doi.org/10.1007/BF00372173.
[9] J. Oliver, Modelling strong discontinuities in solid mechanics via strain softening constitutive equations. Part 2: numerical simulation, Internat. J. Numer. Methods Engrg. 39 (1996) 3601–3623. http://dx.doi.org/10.1002/(SICI)1097-0207(19961115)39:21<3601::AID-NME64>3.0.CO;2-4.
[10] J.M. Melenk, I. Babuška, The partition of unity finite element method: Basic theory and applications, Comput. Methods Appl. Mech. Engrg. 139 (1996) 289–314. http://dx.doi.org/10.1016/S0045-7825(96)01087-0.
[11] T. Belytschko, T. Black, Elastic crack growth in finite elements with minimal remeshing, Internat. J. Numer. Methods Engrg. 45 (1999) 601–620. http://dx.doi.org/10.1002/(SICI)1097-0207(19990620)45:5<601::AID-NME598>3.0.CO;2-S.
[12] N. Moës, J. Dolbow, T. Belytschko, A finite element method for crack growth without remeshing, Internat. J. Numer. Methods Engrg. 46 (1999) 131–150. http://dx.doi.org/10.1002/(SICI)1097-0207(19990910)46:1<131::AID-NME726>3.0.CO;2-J.
[13] N. Moës, T. Belytschko, Extended finite element method for cohesive crack growth, Eng. Fract. Mech. 69 (2002) 813–833. http://dx.doi.org/10.1016/S0013-7944(01)00128-X.
[14] J. Dolbow, N. Moës, T. Belytschko, An extended finite element method for modeling crack growth with frictional contact, Comput. Methods Appl. Mech. Engrg. 190 (2001) 6825–6846. http://dx.doi.org/10.1016/S0045-7825(01)00260-2.
[15] E. Samaniego, T. Belytschko, Continuum–discontinuum modelling of shear bands, Internat. J. Numer. Methods Engrg. 62 (2005) 1857–1872. http://dx.doi.org/10.1002/nme.1256.
[16] S.E. Sanborn, J.H. Prévost, Frictional slip plane growth by localization detection and the extended finite element method (XFEM), Int. J. Numer. Anal. Methods Geomech. 35 (2011) 1278–1298. http://dx.doi.org/10.1002/nag.958.
[17] J. Réthoré, R. de Borst, M.-A. Abellan, A two-scale approach for fluid flow in fractured porous media, Internat. J. Numer. Methods Engrg. 71 (2006) 780–800. http://dx.doi.org/10.1002/nme.1962.
[18] A.R. Khoei, E. Haghighat, Extended finite element modeling of deformable porous media with arbitrary interfaces, Appl. Math. Model. 35 (2011) 5426–5441. http://dx.doi.org/10.1016/j.apm.2011.04.037.
[19] T. Mohammadnejad, A.R. Khoei, Hydro-mechanical modeling of cohesive crack propagation in multiphase porous media using the extended finite element method, Int. J. Numer. Anal. Methods Geomech. 37 (2013) 1247–1279. http://dx.doi.org/10.1002/nag.2079.
[20] S. Mohammadi, Extended Finite Element Method: For Fracture Analysis of Structures, John Wiley & Sons, 2008.
[21] N. Sukumar, D.L. Chopp, N. Moës, T. Belytschko, Modeling holes and inclusions by level sets in the extended finite-element method, Comput. Methods Appl. Mech. Engrg. 190 (2001) 6183–6200. http://dx.doi.org/10.1016/S0045-7825(01)00215-8.
[22] S. Pietruszczak, On homogeneous and localized deformation in water-infiltrated soils, Int. J. Damage Mech. 8 (1999) 233–253. http://dx.doi.org/10.1177/105678959900800302.
[23] S. Pietruszczak, E. Haghighat, Modeling of deformation and localized failure in anisotropic rocks, Internat. J. Solids Struct. (2015).
[24] B. Moran, C.F. Shih, A general treatment of crack tip contour integrals, Int. J. Fract. 35 (1987) 295–310. http://dx.doi.org/10.1007/BF00276359.
[25] S. Bordas, P.V. Nguyen, C. Dunant, A. Guidoum, H. Nguyen-Dang, An extended finite element library, Internat. J. Numer. Methods Engrg. 71 (2007) 703–732. http://dx.doi.org/10.1002/nme.1966.
[26] J. Oliver, M. Cervera, O. Manzoli, Strong discontinuities and continuum plasticity models: the strong discontinuity approach, Int. J. Plast. 15 (1999) 319–351. http://dx.doi.org/10.1016/S0749-6419(98)00073-4.
[27] H.L. Ewalds, R.J.H. Wanhill, Fracture Mechanics, Edward Arnold (Publishers), 1984.
[28] J. Dolbow, N. Moës, T. Belytschko, Discontinuous enrichment in finite elements with a partition of unity method, Finite Elem. Anal. Des. 36 (2000) 235–260. http://dx.doi.org/10.1016/S0168-874X(00)00035-4.
[29] M.B. Nooru-Mohamed, Mixed-mode fracture of concrete: an experimental approach. TU Delft, Delft University of Technology; 1992.